J. Fluid Mech. (1989), *vol.* 202, *pp.* 177–200
Printed in Great Britain

Breaking of wind-generated waves: measurements and characteristics

By PAUL A. HWANG†, DELUN XU‡ AND JIN WU
Air–Sea Interaction Laboratory, College of Marine Studies, University of Delaware, Lewes, DE 19958, USA

(Received 21 December 1987 and in revised form 16 September 1988)

A method of using local wave properties to provide a detailed description of breakings in a random wave field is developed. These properties, derived through the Hilbert transform, include the angular frequency, phase velocity, and surface-velocity components. The breaking characteristics are presented, including the probability of breaking, its time- and lengthscales, its intensity, and the phase of its inception. The time- and lengthscales of breaking events were found to be linearly proportional to the corresponding scales of underlying waves, and to indicate that the breaking region is geometrically similar. Consistent results were obtained from temporal and spatial measurements. Finally, on the basis of these results we have evaluated geometric and kinematic criteria for identifying breaking waves.

1. Introduction

Breaking of water waves is an important phenomenon in many fields of study, including air–sea interaction, remote sensing, wave dynamics, and ocean engineering. It causes separation of airflows from waves (Banner & Melville 1976), induces drastic changes of sea-surface roughness (Wu 1975; Melville 1977) and consequently of the distribution of wind stress along the wave form (Phillips & Banner 1974; Gent & Taylor 1976). Breaking seen as whitecaps (Monahan 1971) is also a source of generating turbulence (Phillips 1977) and entraining air into a water column (Koga 1982); air bubbles have significant effects on gas transfer across the air–water interface (Merlivat & Memery 1983), and produce sea spray (Blanchard & Woodcock 1957). These surface and subsurface features have been closely associated with oceanic remote sensing and underwater acoustic transmission (Medwin 1977; Zheng *et al.* 1983; Banner & Fooks 1985). The turbulence induced by breaking waves in the surf zone is an important mechanism of generating nearshore circulation, and governs the sediment transport (Longuet-Higgins 1970*a*, *b*). Wave breaking also contributes greatly to wave forces acting on offshore structures and ships (Longuet-Higgins 1974; Mogridge & Jamieson 1980); it is the main source of wave-energy dissipation, and affects diffusion, mixing, and dispersion processes in the near-surface ocean.

Observation and quantification of wave breaking, however, have remained a difficult task, and were largely restricted to nearshore or laboratory studies of monochronic waves (Peregrine & Svendsen 1978; Stive 1980; Stive & Wind 1982; Battjes & Sakai 1981). Detailed flow structures under breaking waves were measured in these investigations to understand turbulence generated by the breaking process.

† Present address: Ocean Research & Engineering, Pasadena, CA 91101, USA.
‡ Present address: Ocean University of Qingdao, Qingdao, Shandong, China.

For a simulated breaking wave, Duncan (1981, 1983) photographed and studied the characteristics of an active breaking region; he also associated the breaking-induced drag with the breaking region. Subsequently, Ochi & Tsai (1983) presented the breaking occurrence of laboratory-generated random waves; the breaking probability was shown to be related to the fourth moment of the wave spectrum. Srokosz (1986) adopted a slightly different approach and reproduced the solution of Ochi & Tsai in a simpler form. Snyder, Smith & Kennedy (1983) conducted field measurements of whitecaps and related them to breaking through a statistical model (Snyder & Kennedy 1983); in addition to the breaking probability, spatial and temporal scales of whitecap patches were also reported, and the relationship between the probability of breaking and the fourth moment of the wave spectrum was again verified.

Longuet-Higgins & Smith (1983) were first in using a local parameter for breaking detection. They reasoned that the rise rate divided by the average phase velocity of waves in the record ($R/\bar{c}$) is an indication of the surface inclination, and is therefore a suitable breaking criterion. Xu, Hwang & Wu (1986) slightly modified this idea by replacing $\bar{c}$ with c; the latter is the phase velocity of the wave examined, determined from its zero-upcrossings. In other words, each individual wave defined by the crossings was examined to see if anywhere along its profile the value R/c exceeded the critical slope of 30.37° (Longuet-Higgins & Fox 1977). The probability, duration, and intensity of breaking, all defined in §2.3, were presented by Xu *et al.*, clearly showing that a local variable can be used to provide detailed descriptions of breaking phenomena.

In this article, we have expanded the investigation by using local variables as a tool for detection and quantification of breaking waves; the Hilbert transform was used to generate local variables (Melville 1983; Bitner-Gregersen & Gran 1983). Specifically, we have described the breaking of wind-generated waves in terms of: phase of of breaking inception; breaking probability, duration, and length as well as elevation jump; and multiple breaking occurrences. We have also compared, on the basis of experimental results, breaking characteristics determined with different breaking criteria. These temporal observations of breaking characteristics compare well with the spatial observations of Duncan (1981, 1983) and Snyder *et al.* (1983).

2. Procedures for temporal measurements

2.1. *Derivation of local variables through the Hilbert transform*

To obtain information such as the inception point, duration, and intensity of each breaking event, temporal or spatial measurements are desired. In order to make temporal measurements, local (i.e. instantaneous) wave properties including angular frequency (σ), phase velocity (c), and the horizontal velocity component (u) are needed. These parameters can be deduced through the Hilbert transform (Melville 1983; Bitner-Gregersen & Gran 1983), in which the surface fluctuations are denoted by the following complex representation:

$$\eta(x,t) = \zeta(x,t) + \mathrm{i}\xi(x,t), \tag{1}$$

where $\zeta(x,t)$ and $\xi(x,t)$ are respectively the measured and conjugate signals of vertical

fluctuations of the water surface; x and t are the space and time coordinates, respectively. The quantities ζ and ξ are uniquely defined by the Hilbert transform:

$$\zeta(x,t) = \frac{p}{\pi}\int_{-\infty}^{\infty}\frac{\xi(x,\tau)}{\tau - t}\,\mathrm{d}\tau, \tag{2}$$

$$\xi(x,t) = \frac{p}{\pi}\int_{-\infty}^{\infty}\frac{\zeta(x,\tau)}{\tau - t}\,\mathrm{d}\tau, \tag{3}$$

where p is the Cauchy principle value of integration evaluated at $\tau = t$. From the convolution theorem, we have

$$F(\xi) = \mathrm{i}F(\zeta)$$

where F denotes the Fourier transform. In practical computations, a fast Fourier transform is employed to obtain $\xi(x,t)$ from $\zeta(x,t)$ with a $\frac{1}{2}\pi$ phase shift of each elementary harmonic of $\zeta(x,t)$ (Melville 1983). The complex signal in (1) can be expressed in the polar form as

$$\eta(x,t) = a(x,t)\,\mathrm{e}^{\mathrm{i}\phi(x,t)}, \tag{4}$$

where $a(x,t) + [\xi^2(x,t) + \zeta^2(x,t)]^{\frac{1}{2}}$ is the local wave amplitude, and $\phi(x,t) = \tan^{-1}[\zeta(x,t)/\xi(x,t)]$ is the local phase function. The local wavenumber and angular frequency can then be obtained, respectively, from the following definitions:

$$k(x,t) = \frac{\partial\phi(x,t)}{\partial x}, \tag{5}$$

$$\sigma(x,t) = \frac{\partial\phi(x,t)}{\partial t}. \tag{6}$$

The local wave celerity is defined by

$$c(x,t) = \frac{\sigma(x,t)}{k(x,t)}. \tag{7}$$

Alternatively, Melville (1983) showed that the phase velocity of a narrow-band process obtained from

$$c(x,t) = [g/\sigma(x,t)][1 + (ak)^2] \tag{8}$$

agreed well with (7). In the following application, $k = \sigma^2/g$ is substituted into (8); the phase velocity can then be obtained from single-station measurements to second-order accuracy.

Note that although the above formulation was derived for narrow-band processes, its application to ocean waves appears to result in reasonable success (Bitner-Gregersen & Gran 1983). Finally, local horizontal and vertical velocity components at the free surface can be approximated to first order by finite differencing

$$u(x,t) = \frac{\partial\xi(x,t)}{\partial t}, \tag{9}$$

$$w(x,t) = \frac{\partial\zeta(x,t)}{\partial t}. \tag{10}$$

2.2. *Threshold variables for breaking measurements*

The three most frequently used criteria of wave breaking are:

Kinematic criterion. The wave breaks when the longitudinal particle velocity

exceeds the wave phase velocity ($u/c \geqslant 1$). Since we are interested in large-scale breaking, effects of surface drift currents on breaking will not be considered (Banner & Phillips 1974; Phillips & Banner 1974).

Geometric criterion. Breaking occurs when the surface inclination exceeds 30.37°, or $\partial\zeta/\partial x \geqslant \tan 30.37°$ (Longuet-Higgins & Fox 1977). Following a treatment of rendering local steadiness of wave motions, the surface inclination can be approximated by $\partial\zeta/\partial x = c^{-1}\partial\zeta/\partial t$ (Longuet-Higgins & Smith 1983).

Dynamic criterion. The acceleration of fluid particles exceeds a portion of the gravitational acceleration when the wave breaks. The proportionality constant ranges from 0.388 near the wave crest, based on numerical calculations of Longuet-Higgins & Fox (1977), to the classical value of 0.5 (Stokes 1880). Recent work of Longuet-Higgins (1985) showed that the apparent downward acceleration could be unlimited.

All the quantities involved can be calculated from local parameters derived by the method outlined in the last section. The dynamic criterion involves the second derivative of water-surface displacement; the resulting signal is very erratic owing to not only the discontinuity at the breaking point but also the amplification of noises through differential processes. A similar problem has been commonly encountered in the frequency domain transformation, where high-frequency components are amplified excessively; in this case an artificial upper cutoff frequency must be specified (Snyder & Kennedy 1983; Ochi & Tsai 1983). Our analysis is therefore limited to the first two criteria.

2.3. *Characteristics of wave breaking*

In many recent measurements of breaking waves, only the probability of occurrence was emphasized. For a better description of the breaking process, other quantities characterizing the breaking events should be investigated. These quantities are discussed in the following:

Probability of occurrence. The probability of breaking P_b is defined as the ratio between the number of breaking waves and the total number of waves recorded (Longuet-Higgins & Smith 1983; Xu *et al.* 1986).

Timescale of breaking. The breaking duration ΔT_b, defined as the time interval during which the threshold variable exceeds the critical value (Xu *et al.* 1986), is the most appropriate timescale of breaking.

Lengthscales of breaking. The elevation jump ΔH_b, defined as the difference in surface elevations during breaking (Longuet-Higgins & Smith 1983; Xu *et al.* 1986), is used as the vertical lengthscale of breaking. The horizontal lengthscale can be derived from the measured breaking duration (ΔT_b) and the period of the corresponding breaking wave (T_b). Since $L_b = gT_b^2/2\pi$ is the length of the breaking wave and $\Delta T_b/T_b$ is the phase angle that a breaking patch spans, the quantity $gT_b\,\Delta T_b/2\pi = \Delta L_b$ is therefore the horizontal lengthscale of a breaking patch (Phillips 1985). In dimensionless forms, $\Delta L_b/L_b$ is identical to $\Delta T_b/T_b$; both represent the phase span of a breaking patch.

Intensity of breaking. Although this appears to be the most interesting quantity, a precise definition does not seem to be easy. We shall tentatively relate this quantity to the following two measurable, or calculable, properties: the elevation jump ΔH_b as an index of the prospective potential-energy loss and $\Delta Q_b = u^2 + w^2$ as the kinematic-energy loss during breaking, where u and w are respectively the longitudinal and vertical components of the particle velocity at the free surface calculated from (9) and (10). Duncan (1983) demonstrated that the drag associated

with breaking was closely related to the weight of water in the breaking region. In a later section, we shall show that this weight is proportional to the jump height.

Phase of breaking inception. The phase of breaking is indicated by the phase angle (θ_b) relative to the wave crest of the first point where the threshold variable exceeds the critical value.

Multiplicity of breaking. There is generally only one breaking event per wave; occasionally, two or more breakings occurring at different phases were observed. The significance of this is not clear at this stage, but is useful in comparing different breaking criteria. Because the wave profile is very complicated at the breaking point, some of the multiple-breaking events occurring in close proximity may be due to the difficulty of measurements. Therefore, when two events were separated by only a short time, say 0.01 s corresponding to roughly one time interval in digitization, they were considered as one event. The multiplicity of breaking (M_b) is defined here as the number of breaking events divided by the number of breaking waves.

With point measurements, breaking events detected by the probe may be at various stages of development, ranging from just initiated, through fully developed to nearing the end of receding. Such conditions also apply to spatial observations. At any instant, the breaking events recorded over a large area constitute all stages of maturity. The time- and lengthscales measured by either method, therefore, do not represent the corresponding quantities for a fully developed stage but the ensemble means of those properties over the whole lifetime of the breaking process. Alternatively, space–time measurement over a small area (e.g. Snyder *et al.* 1983) are capable of recording the evolution of a breaking event. Such measurements can provide information on the lifetime of the breaking wave and lengthscales at various stages of the breaking development. In the following, breaking duration and length are used to describe the two scales at full development; the corresponding quantities obtained by our point measurements are simply called time- and lengthscales.

3. Results

Experiments were carried out in the Wind-Wave-Current Research Facility. The range of wind velocities covered in this experiment was from 7 to 16 m/s ($36 < u_* < 138$ cm/s, where u_* is the friction velocity). Profiles of wind-generated waves at a fetch of 20 m were measured with a capacitance probe and recorded for analysis. Details of the facility and experiments have been reported in (Xu *et al.* 1986).

Segments of time series of $\zeta, \xi, \partial\zeta/\partial x = \partial\zeta/\partial t/c$, and $u/c = \partial\xi/\partial t/c$ at the wind velocity of 16 m/s are shown in figure 1; from visual observations, nearly every wave broke at this wind velocity. The breaking event can be easily detected in figure 1. In the ζ-plot, the breaking event appears as a sudden jump in the surface elevation; this is even more obvious in the plot of u/c or $\partial\zeta/\partial x$, where abrupt increases are seen. The data were digitized at a rate of 128 samples/s to preserve features of surface jump. To reduce noise effects, the sampled data were low-pass filtered at 14 Hz; low-passing at a lower frequency would distort jump features.

3.1. *Phase of breaking inception*

The phase, leading the wave crest, of breaking inception is of interest in the understanding of breaking phenomena. In terms of the kinematic criterion, this position represents the stagnation point of the streamlines of fluid particles relative to the wave form. Downstream from this point, fluid particles tend to escape from

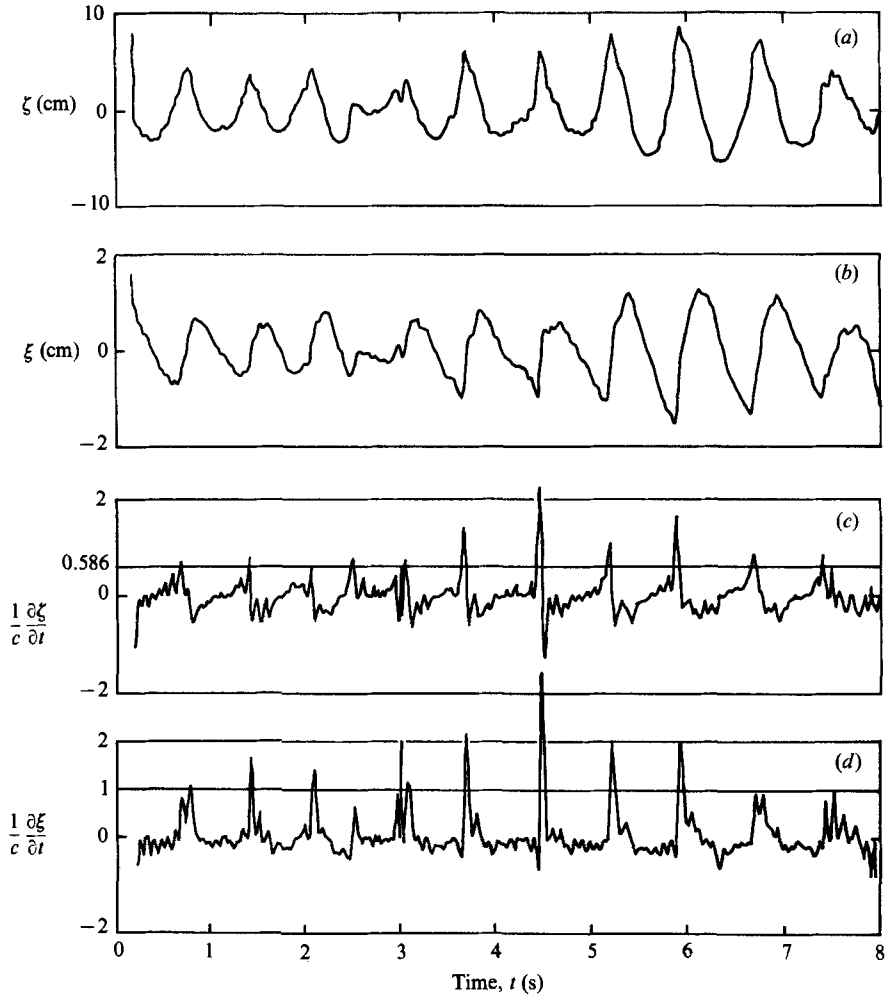

FIGURE 1. Sample data. Time series of (*a*) surface elevation ζ, (*b*) conjugate signal ξ, (*c*) breaking variable $\partial\zeta/\partial x$ approximated by $\partial\zeta/\partial t/c$, and (*d*) breaking variable u/c approximated by $\partial\xi/\partial t/c$. The wind velocity was 16 m/s, and the waves were measured at the fetch of 20 m.

the water surface; they can either be ejected into the air to become droplets, or curl down to trap air into water. Such events are closely associated with exchanges of mass, momentum and energy across the air–water interface. Whereas from the geometric criterion, the wave profile becomes locally unstable with patches of water starting to detach from the wave profile, the wave breaks. Two phase angles are of interest here: the first angle in temporal sequences is the downstream edge of the breaking patch denoted as θ_ℓ, and the last angle is the upstream edge, θ_t. In other words, quantities θ_ℓ and θ_t represent respectively the leading and trailing edges of the breaking patch in a temporal sequence caught by the wave probe. Although there are some doubts that either of these phases measured by a fixed probe represent the true point of inception, there is ample evidence in the figures and picture sequences presented in Longuet-Higgins (1974) and Snyder *et al.* (1983) to indicate that the trailing edge remained close to the inception point of breaking. This is also pictured in the 'entraining plume' model proposed by Longuet-Higgins & Turner (1974). In

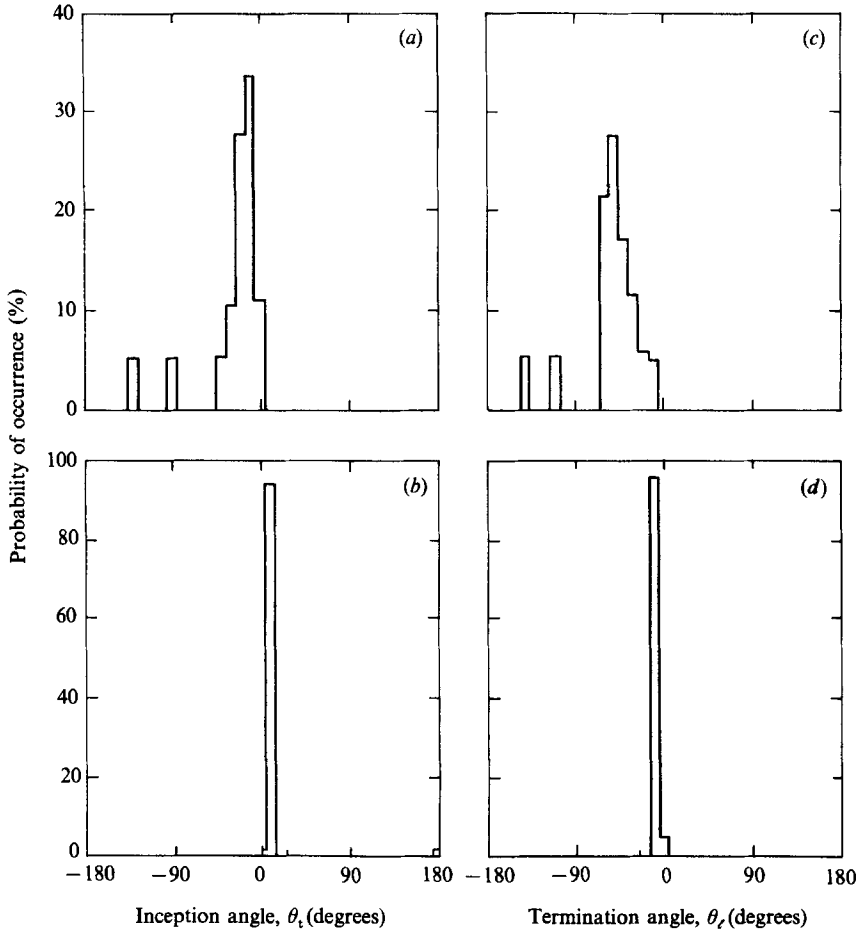

FIGURE 2. Probability distributions of breaking phases. The inception (trailing) edge of breaking patches is shown in (*a*, *b*) and the termination (leading) edge in (*c*, *d*). Zero degree is at the wave crest, and the positive phase is in the upwind direction. The data were obtained at the wind velocity of 7 m/s with the geometric (*a*, *c*) and kinematic (*b*, *d*) criteria.

the following, we therefore consider the trailing phase θ_t as the angle of breaking inception θ_b. The probability distributions of the inception phase at the wind velocity of 7 m/s are shown in figure 2(*a*, *b*), where zero degree corresponds to the wave crest and the negative value is on the downwind side. Inception of breaking below the mean water level was detected occasionally; this is the second type of breaking, with short waves breaking on long carrier waves as discussed in Xu *et al.* (1986). Distributions of the leading phase of breaking are shown in figure 2(*c*, *d*). The most probably breaking inception is seen to occur near the wave crest, and the leading edge of a breaking patch occurs mostly on the downwind side of a wave crest. There appears to be less variation in the trailing phase than in the leading phase. This is consistent with the observation discussed above that the trailing edge of breaking patch remained near the breaking inception. The difference between θ_ℓ and θ_t, a measure of the size of the breaking patch, is directly related to the dimensionless breaking duration, and will be further discussed in §3.4.

Phase angles of the most probably occurrences of θ_ℓ and θ_t at different wind-friction velocities are shown in figure 3. A trend of wave breaking moving closer to

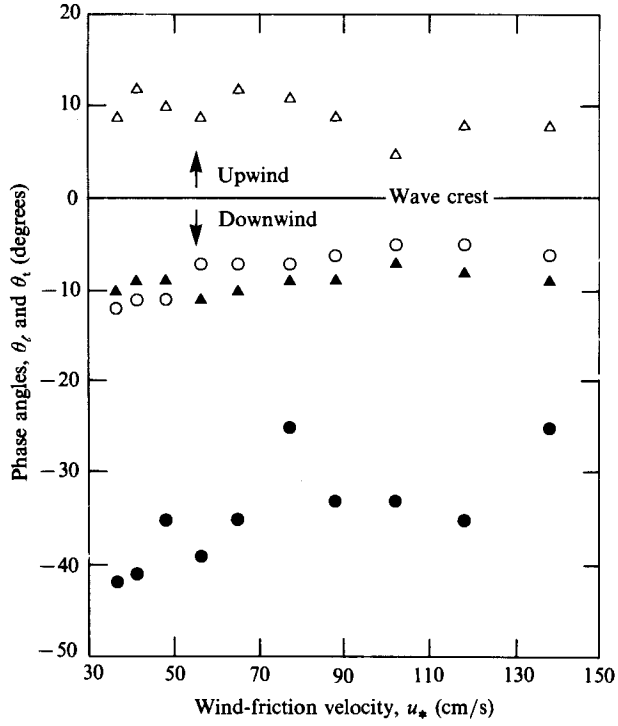

FIGURE 3. Phases of inception (trailing angle) and termination (leading angle) of breaking at different wind-friction velocities. The data analysed with the geometric criterion are indicated by ○, and the kinematic criterion by △; open symbols are for inception angle, and solid symbols for termination angle.

the wave crest at higher wind velocities is demonstrated in the figure. It is quite interesting to observe that, based on the geometric criterion, the breaking inception is on the downwind side of the wave crest, while the kinematic criterion indicates inception on the upwind side. This delicate difference, although restricted to a narrow region of $\pm 10°$ of the wave crest, demonstrates that the breaking phenomena described by these two criteria, as well as by other threshold variables, are not exactly the same. This figure also shows that in temporal wave measurements the surface profile steepens beyond the critical level (the geometric criterion) earlier than when the particle velocity exceeds the phase velocity (the kinematic criterion). In spatial measurements, however, these two criteria may trigger breaking simultaneously.

3.2. *Probability of breaking*

The probability of breaking of wind waves based on local criteria is presented, versus the friction velocity, in figure 4(*a*). It is seen that although the magnitudes of P_b differ for two criteria of breaking, their rates of increase with wind velocity are similar. In the present laboratory study, the breaking probability for wind velocities from 7 to 16 m/s ranges from 7 to 10% based on the geometric criterion, and from 5 to 50% on the kinematic criterion. In other words, the geometric criterion is seen to be more sensitive in detecting breaking events. The breaking probability obtained with the geometric instability is on average 1.4 times higher than that with the kinematic instability. Alternatively, we show the frequency of breaking occurrence (n_b) in figure 4(*b*). The data represent the average number of breaking waves per second

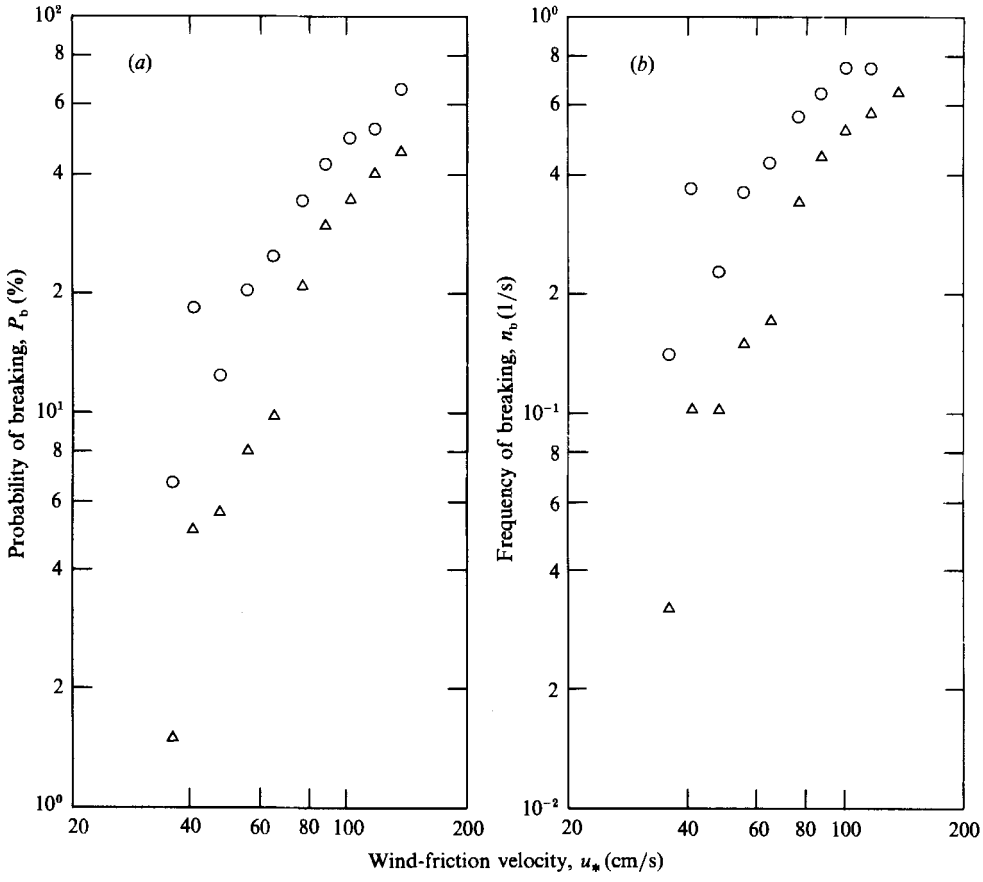

FIGURE 4. (*a*) Probability and (*b*) frequency of breaking occurrence at various wind-friction velocities. The data analysed with the geometric criterion are indicated by ○, and the kinematic criterion by △.

observed during a period of 128 s. Both probability and frequency of breaking increase rapidly with u_* under light winds ($u_* < 80$ cm/s); the rate of increase slows down sharply under high winds.

Further inspection of breaking waves detected by the two criteria reveals that there were significant portions of events detectable by one criterion but not by the other. Consequently, a parameter is used to indicate the differential detectability, D_{ij}, where i denotes the criterion that detects breaking, and j the criterion that detects no breaking; the subscripts i and j can be either g or k for the geometric and kinematic criteria, respectively. The results at various wind-friction velocities are presented in figure 5, confirming that the geometric criterion is a more sensitive breaking indicator. Except for two data points, D_{kg} is generally less by 14%, indicating that over 86% of breaking waves classified by the kinematic criterion are also identified by the geometric criterion. The linear increase of D_{gk} from about 30% at 16 m/s ($u_* = 138$ cm/s) to 80% at 7 m/s ($u_* = 36$ cm/s) also shows that the kinematic criterion is less sensitive, especially at lower wind velocities.

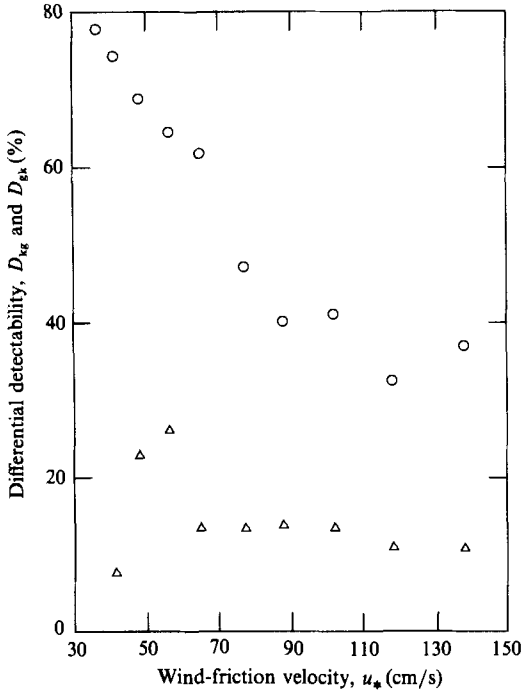

FIGURE 5. Differential detectabilities at various wind-friction velocities. ○, D_{gk}; and △, D_{kg}.

3.3. *Breaking repetition*

The index of multiple breaking is presented in figure 6; it increases linearly with the wind velocity. The probability of multibreaking events was found to be about 20% more at the highest wind velocity (16 m/s) than at the lowest (7 m/s) for the geometric criterion, and about 10% for the kinematic criterion. The increase of the measured multiple breaking events is undoubtedly associated with the fact that wind-generated waves are rougher at higher wind velocities.

3.4. *Breaking duration*

The timescale of breaking ΔT_b is shown in figure 7(*a*); it is of the order of 30 ms. The magnitudes determined with the two criteria are different. With the geometric criterion, ΔT_b increased from 29 ms at low (7 m/s) to 45 ms at high (16 m/s) winds; the results based on the kinematic criterion show a similar trend, but the duration is generally 5–7 ms shorter. These results indicate that the breaking event is highly transient and occurs in a very short time span. Normalized by the period of the corresponding breaking wave, the dimensionless breaking duration is seen in figure 7(*b*) to be approximately constant, generally about 4–6%, depending on the method of breaking measurements.

3.5. *Breaking length*

Figure 8 plots ΔL_b versus u_*. Regardless of quantitative differences of ΔL_b determined with geometric and kinematic considerations, both measurements show that ΔL_b increases with u_*, and is proportional to the length of the breaking wave as illustrated in figure 7(*b*), noting that $\Delta L_b/L_b = \Delta T_b/T_b$.

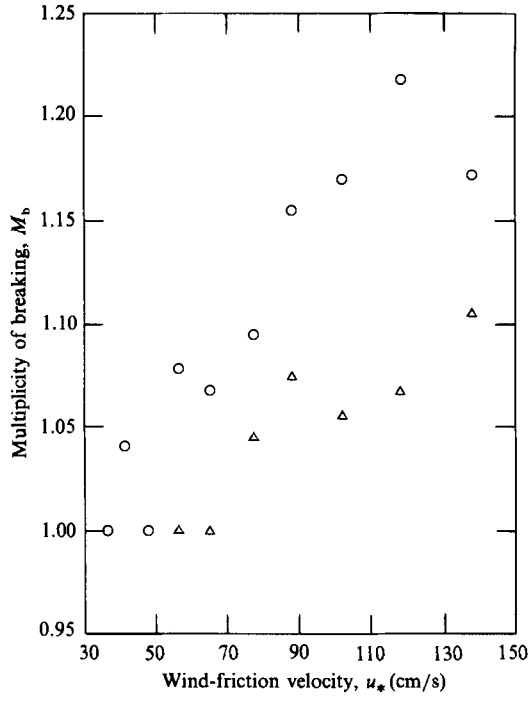

FIGURE 6. Multiplicity of breaking at various wind-friction velocities. Symbols are as in figure 4.

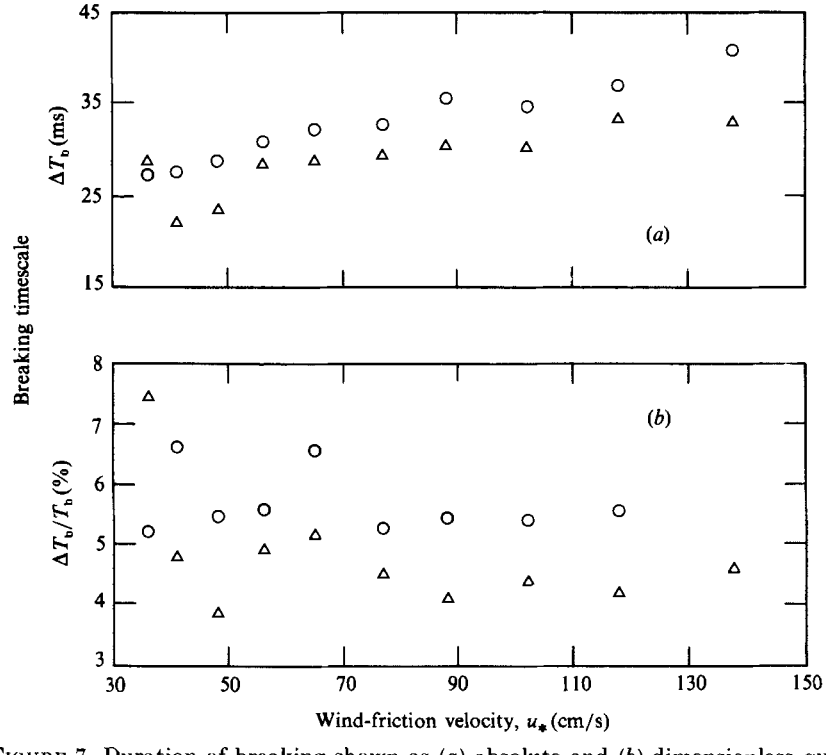

FIGURE 7. Duration of breaking shown as (*a*) absolute and (*b*) dimensionless quantities. Symbols are as in figure 4.

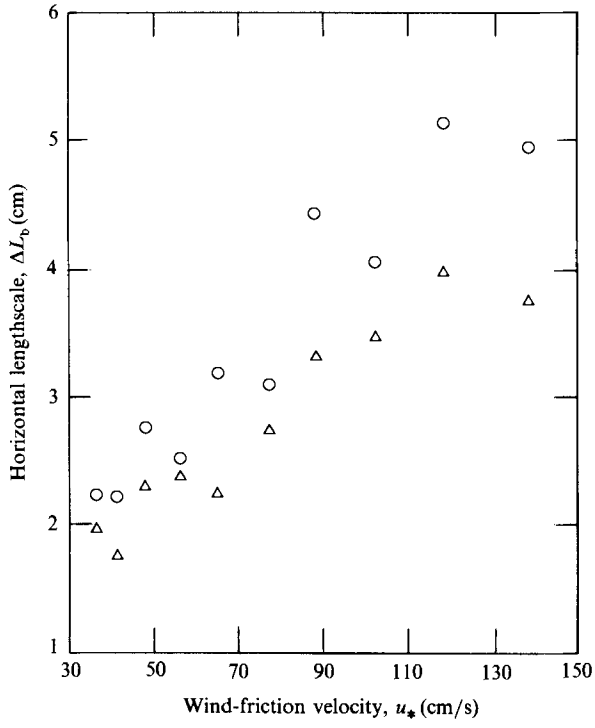

FIGURE 8. Horizontal lengthscale calculated from breaking duration as a function of wind-friction velocity. Symbols are as in figure 4.

3.6. *Breaking height and intensity*

In the last section, we proposed to relate the intensity of breaking to the potential- or kinetic-energy loss. Not all water particles qualified for breaking, however, detach from the water surface; furthermore, it is not known to which elevation those detached particles would fall. Intuitively as well as logically, we chose ΔH_b and ΔQ_b as prospective potential- and kinetic-energy losses, respectively; their dependences on the wind-friction velocity are shown in figures 9(*a*) and 10(*a*). The increase of both energy losses with the wind velocity is quite evident. The magnitude of ΔH_b measured by the kinematic criterion is much smaller than that by the geometric criterion, as a consequence of a much later breaking inception and an earlier termination illustrated in figures 2 and 3. The kinetic-energy loss ΔQ_b measured with the kinematic criterion is, however, greater. This difference is significant, since the kinematic criterion measured a much shorter breaking duration but closer to the wave crest; see figures 3 and 7. They illustrate that the kinetic energy at the crest is considerably higher than at other phases of breaking waves. Note that for small-amplitude waves, $\Delta Q = u^2 + w^2$ is proportional to $\cos^2\theta + \sin^2\theta$, and should have a constant value regardless of the phase of measurements. Results from Duncan's (1983) experiments also indicated that there was a significant difference in wave drag between breaking and non-breaking waves. Figures 9(*b*) and 10(*b*) are respectively dimensionless plots for ΔH_b and ΔQ_b normalized by the corresponding global quantities of the individual breaking waves, i.e. the wave height and the total kinetic energy integrated over the whole breaking wave, respectively. Figures 9 and 10 represent a likely upperbound estimate of the wave-energy loss due to breaking. As shown in figure 9(*b*), the normalized breaking

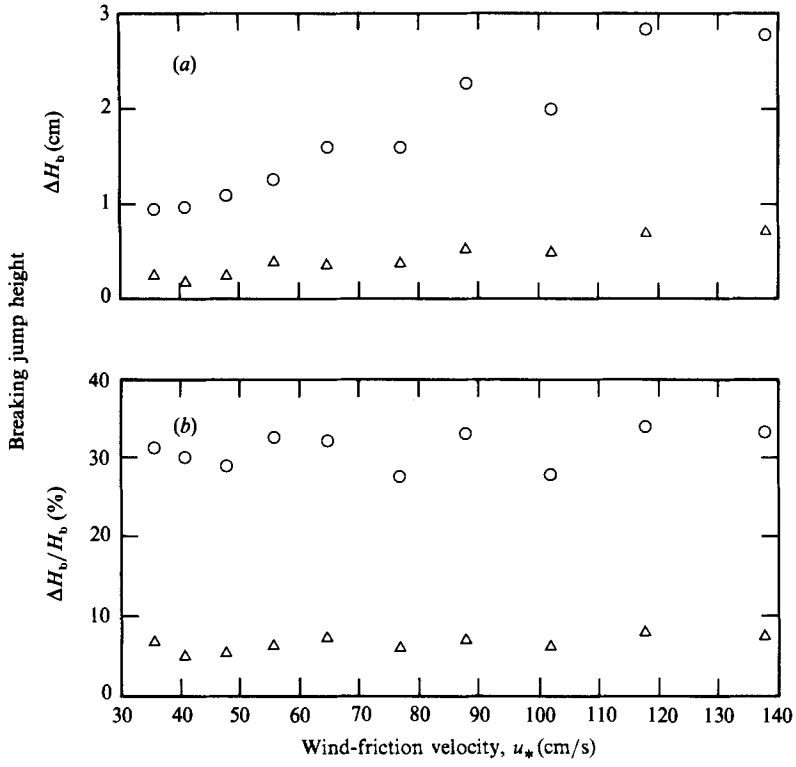

FIGURE 9. Breaking intensity in terms of surface jump height in (*a*) dimensional and (*b*) dimensionless magnitudes. Symbols are as in figure 4.

intensity $\Delta H_b/H_b$ is nearly constant ($30\pm3\%$ from the geometric criterion, $6\pm2\%$ from the kinematic criterion). The magnitudes of $\Delta Q_b/Q_b$ are generally in the range between 20 and 25%, with a larger scatter of data analysed with the kinematic criterion.

4. Discussion

4.1. *Breaking probability*

Previous studies (Snyder & Kennedy 1983; Ochi & Tsai 1983) show that the probability of breaking is closely related to the truncated fourth moment of the wave spectrum, which can be interpreted as either the acceleration or the wave-slope spectrum. In figure 11(*a*), we present the calculated mean-square slope, $(\nabla\zeta)^2 = \overline{(\partial\zeta/\partial t/c)^2}$, where the overbar denotes the time average, versus the wind velocity. The smoothed curve $(\nabla\zeta)^2 = 1.35\times10^{-3}U^{\frac{5}{3}}$ is used to plot P_b versus $(\nabla\zeta)^2$ in figure 11(*b*). The breaking probability derived from both geometric and kinematic criteria shows a significant dependence on the mean-square slope; this trend is consistent with the results of Ochi & Tsai (1983), shown as a solid curve in the figure. Srokosz (1986) reproduced the solution of Ochi & Tsai (1983) in a considerably simplified form: $P_b = \exp[-\alpha^2/2(\nabla\zeta)^2]$, where α is the ratio between the downward acceleration at the wave crest and the gravitational acceleration. The breaking criterion $H/gT^2 = 0.02$ adopted by Ochi & Tsai, corresponds to $\alpha = 0.4$. A more classical value of $\alpha = 0.5$ shown as a dashed line in figure 11(*b*) provides a closer agreement with the present

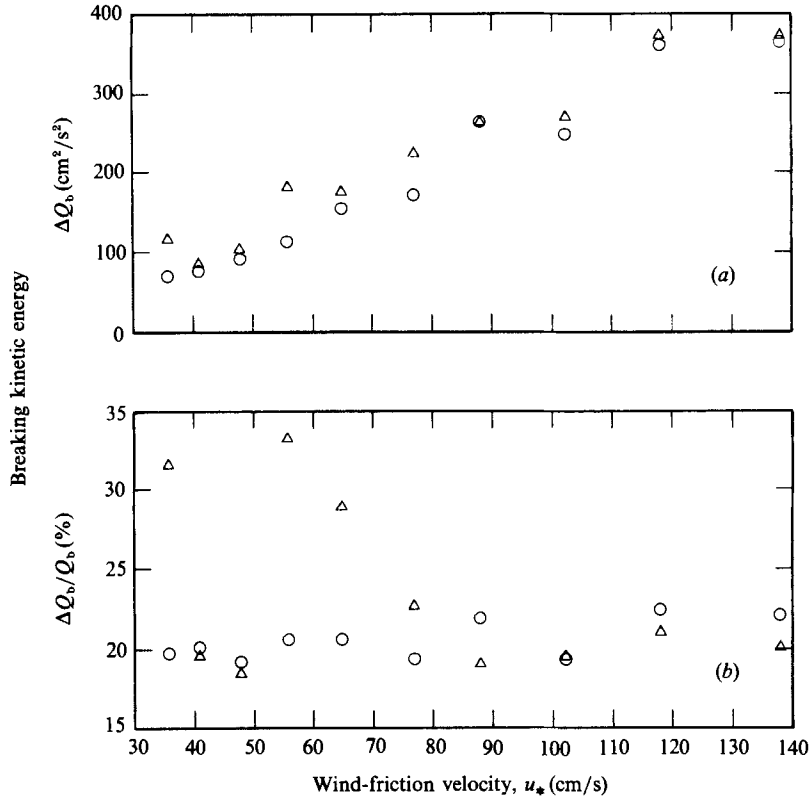

FIGURE 10. Breaking intensity in terms of kinetic energy in (*a*) dimensional and (*b*) dimensionless magnitudes. Symbols are as in figure 4.

data. Note that in order to calculate the fourth moment, it is necessary to specify an upper cutoff frequency to assure convergence in the computation; consequently, the magnitude of the breaking threshold based on the fourth moment is generally affected by the choice of cutoff frequency. Furthermore, Longuet-Higgins (1985) studied the apparent and real accelerations in steep gravity waves and disagreed with both numbers cited above for α; this is discussed further in §4.6.

Snyder *et al.* (1983) conducted photographic experiments on wave breaking and whitecaps. Their estimate of breaking probability at a given point, or the fraction of surface covered by breaking water, is of the order of 10^{-4} for wind velocities in the range from 2 to 9 m/s. This quantity is comparable with the present result of $P_b(\Delta L_b/L_b)^2$. From their tabulated results on whitecaps, we calculated the ratio between the number of (complete) whitecap events and that of breaking waves. If there is a one-to-one relationship between whitecaps and breaking waves, this ratio will be nearly the same as the breaking probability as defined in the present experiment. Although the field data are more scattered, similarities in terms of both magnitudes and dependence on the wind velocity are displayed by both sets of data in figure 12.

Phillips (1985) derived a theoretical expression for the frequency of breaking occurrence (n_b) of waves with phase velocity in the range (c_0, c_1)

$$n_b(c_0, c_1) \sim u_*^3 g c_0^{-4}[1-(c_0/c_1)^4]. \tag{11}$$

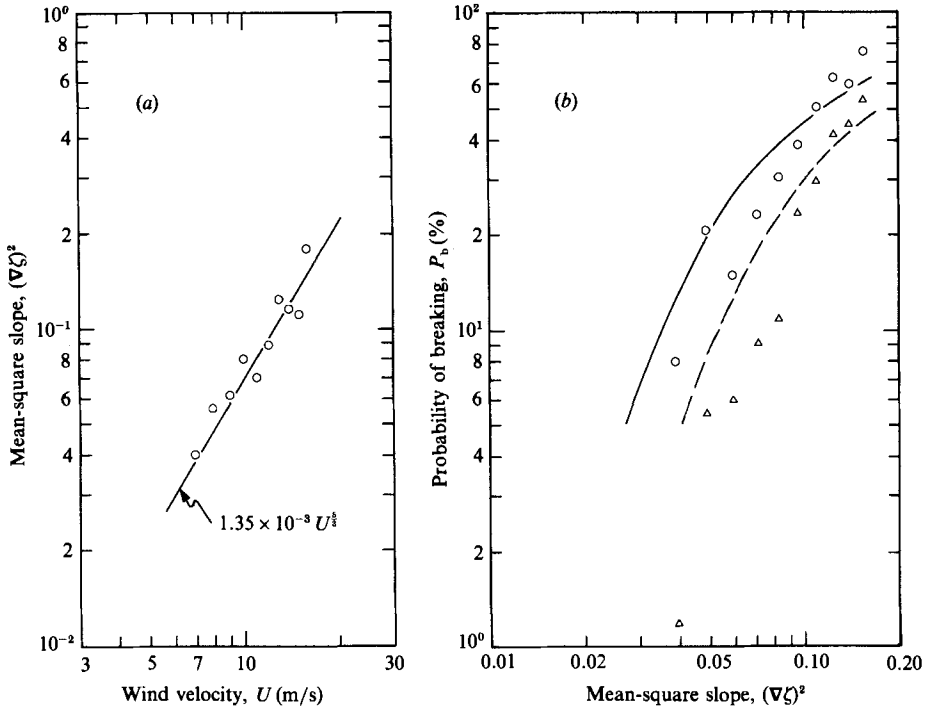

FIGURE 11. Mean square slope and breaking probability. The results are determined with the geometric (○), and kinematic (△) criteria; the solid curve represents the results of Ochi & Tsai (1983), and the dashed curve is the solution of Srokosz (1986) for $\alpha = 0.5$.

To apply this equation to our observation, we can take c_0 as the minimum phase velocity corresponding to waves at about 13 Hz in the absence of current, which is roughly the upper limit of our wave-probe frequency response; and c_1 as the phase velocity of waves at the peak frequency of the spectrum. The introduction of (c_0, c_1) into the formulation implied that the u_* dependence of n_b will vary at different wind velocities since c_0/c_1 increases as u_* decreases; the u_* dependence of n_b at low winds should be greater than at high winds (O. M. Phillips 1988, private communication). This qualitative trend was indeed observed; see figure 4(*b*). Quantitatively, however, the range of c_0/c_1 measured in our experiments is between 0.2 and 0.3. The dependency $n_b \sim u_*^3$ is predicted in (11) for the whole range of wind velocities. The present data is better fitted with $n_b \sim u_*^{2.64}$ for $u_* < 80$ cm/s and $n_b \sim u_*^{1.0}$ for higher winds.

4.2. *Breaking duration*

Direct measurements of breaking duration were very scarce. Searching through related works in ocean engineering, we found that the impact duration of a breaking wave on a structure appeared to be closely related to the breaking duration. The impact force on a structure generally constitutes two components, the so-called hammer shock caused by the piling of the wave crest on the structure, and the compression shock by the air trapped by breaking (Mogridge & Jamieson 1980). The hammer shock produces a large impact of a very short duration, in order of 1 to 10 ms (Mogridge & Jamieson 1980; Wiegel 1982). The compression shock is typically a series of successively damped oscillations of the wave force created by a trapping–release process of air and the structure elasticity. Mogridge & Jamieson

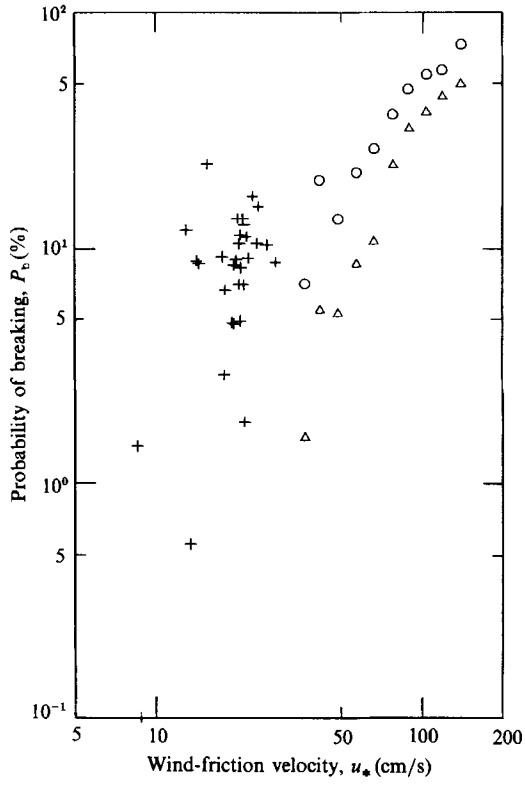

FIGURE 12. Comparison of the probability of whitecap events (+, Snyder *et al.* 1983) and the probability of breaking determined with geometric (○) and kinematic (△) criteria.

measured the wave force on a solid-wall breakwater by waves having a period of about 2.1 s. Their results showed that the period of oscillation of the compression force was about 40 ms or 2% of the wave period. Since the air trapping is caused by a sudden rise of the water surface and the subsequent curling down of the wave form, the oscillation period of the compression force is directly related to the breaking duration, ΔT_b. Based on the limited results of Mogridge & Jamieson, it is estimated that the oscillation period of the compression force is about 40 to 50% of the breaking duration. The breaking duration is therefore about 80 ms, or 4% dimensionlessly, being in good agreement with the present study.

Snyder *et al.* (1983) measured the average duration and sweep area of whitecaps. Their data were processed to derive the time- and lengthscales of breaking events, the latter is taken as the square root of the sweep area. These scales are surprisingly, seen in figure 13, to be independent of either the wind velocity or the corresponding time- and lengthscales of wave fields (wave period and length, respectively). The results indicate that whitecaps have a constant timescale of about 0.5 s and a lengthscale of approximately 1 m in a wind-generated sea; there will be more discussion of these observations in a later section.

4.3. *Breaking lengthscales*

The breaking height and length are respectively the vertical and horizontal lengthscales of breaking waves. We have shown that both scales increase with the wind velocity and are proportional linearly to the height and length of waves, shown

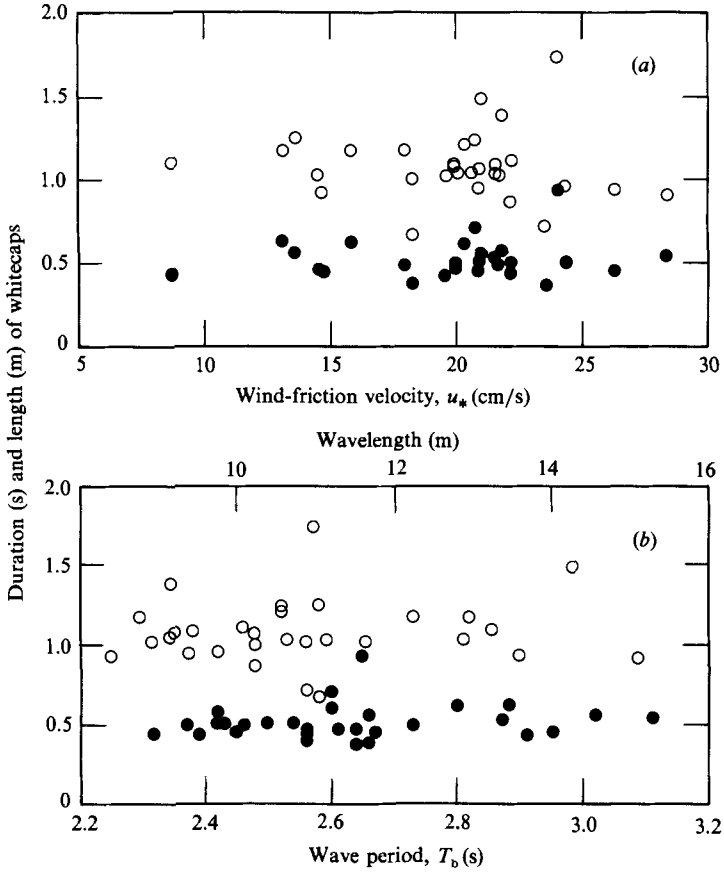

FIGURE 13. Time- and lengthscales of whitecaps as a function of (*a*) wind-friction velocity, and (*b*) wave period and length. The data are from Snyder *et al.* (1983). Timescale is indicated with solid circles, and lengthscale with open circles.

respectively in figures 8 and 9. Duncan (1981) investigated quasi-steady breaking waves simulated by a towed hydrofoil, and reported the geometry of the breaking region, which he defined as the 'zone of turbulent water', riding on the forward slope of breaking waves. Duncan's data on variations of the vertical lengthscale with the wave height are shown in figure 14. A fourth vertical scale defined in a curvilinear sense as the ratio between the area and the length of the breaking region in the direction tangential to the water surface was also calculated from Duncan's data; see figure 14. The magnitude of the last scale is very close to the jump height measured by the geometric criterion.

Horizontal lengthscales of breakers at various wavelengths from both Duncan's and the present experiments are presented in figure 15. The breaking lengthscales derived from spatial and temporal measurements are obviously proportional to each other.

Since the ratio H_b/L_b is about constant for breaking waves of either a monochromatic wavetrain or in a random wave field (Michell 1893; Ochi & Tsai 1983; Xu *et al.* 1986), one consequence of the scale of breakers being proportional to that of waves is the linear proportionality between the vertical and horizontal lengthscales of the breaking area; see figure 16. This further suggests a geometrical

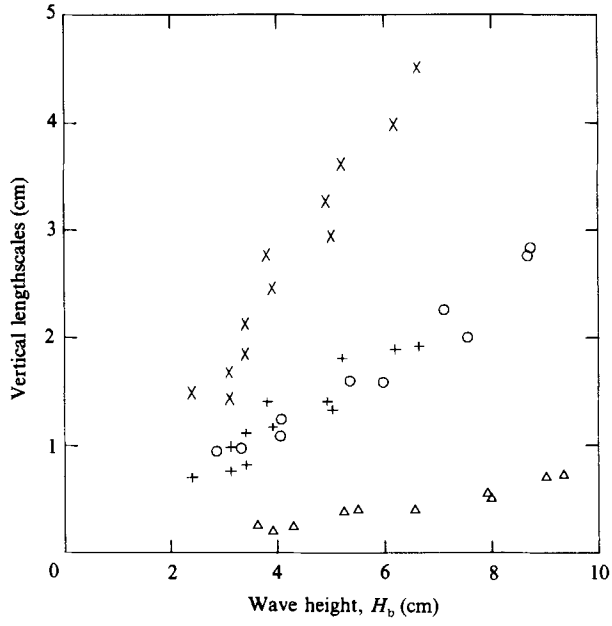

FIGURE 14. Variation of vertical lengthscale with wave height. The symbols are: present experiment, geometric (○) and kinematic (△) criteria; Duncan's (1981) data, vertical dimension of the breaking region (×) and the ratio between the area and tangential length of the breaking region (+).

similarity of breakings expressed either as 'a zone of turbulent water' as in Duncan's experiment, or 'a region that exceeds certain threshold criteria' as in the present measurements. Furthermore, the quasi-steady breakers of Duncan's experiment can be considered as a fully developed breaking patch, while our measurements are averaged over various stages of the breaking development as discussed previously. The implications of similarity at various stages of breaking, and the extension of similarity to wind-wave fields are important in the understanding of the breaking processes. This geometrical similarity further strengthens the suggestion that the breaking jump height is a proper indicator of breaking intensity. This of course also receives some support from Duncan's drag measurements relating the breaking drag to the vertical dimension of the breaking region.

4.4. *Laboratory and field conditions*

In previous sections, we have compared our point measurements of breaking characteristics with two sets of spatial breaking observations. There is substantial agreement between Duncan's (1981, 1983) and our results in terms of the vertical and horizontal lengthscales of breaking events; both increase linearly with the corresponding lengthscales of the underlying waves. This encouraging result provides evidence that the transient breaking characteristics, which so far can only be detailed by visual description and tedious photographic processing, can also be provided by point measurements. The significance of such convenience in breaking observations cannot be discounted.

The whitecap observations of Snyder *et al.* (1983), however, displayed considerably different breaking characteristics in the ocean. Specifically, the timescale and the horizontal lengthscale of whitecap patches are nearly constant (figure 13). When we

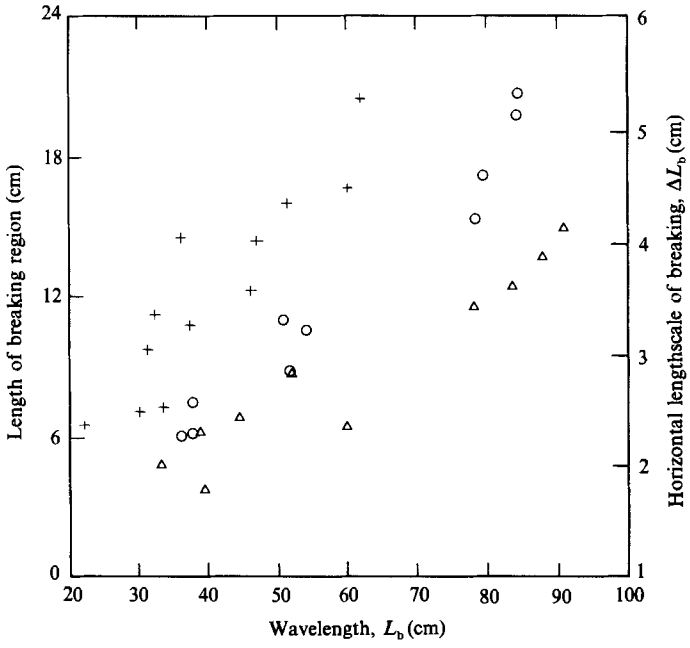

FIGURE 15. Variation of horizontal lengthscale with wavelength. The data are from the present experiment determined with geometric (○) and kinematic (△) criteria; and from Duncan's (1981) horizontal dimension of the breaking region (+).

first compared their results with our breaking measurements (figures 7, 8, 13), it was quite tempting to attribute the discrepancy to the different parameters observed. Subsequent comparison of our results with Duncan's spatial measurements (figures 14, 15, 16), however, showed a close agreement of breaking scales. Since the observation of Duncan's 'zone of turbulent water' is possibly equivalent to the whitecap patch in the context of Snyder *et al.*, the difference in the characteristic length- and timescale can not be attributed to the different quantities observed. There are at least two feasible explanations to this puzzling outcome. First, the growth of whitecaps is critically controlled by flow conditions, to which wave motions contribute significantly. Whitecaps observed in a wind-wave tank are generally younger, owing to limited fetches, while a much longer wave period in the field allows the whitecap to develop to a more mature stage. Observations showed that the lifetime of bubbles in the 1 mm diameter range is longer than 1 s (Burger & Blanchard 1983). In comparison, the wave period in Duncan's and the present experiments is about 0.5 s, the wave in the experiment of Snyder *et al.* is about 3 s. Secondly, regardless of timescales of the oscillatory flow field, there appear to exist major differences in decay rates of small bubbles in fresh and salt waters. Monahan & Zietlow (1969) demonstrated that under the same simulated breakers, fresh-water bubbles of diameter 500 μm and smaller diminish much faster than those of salt water. The ability of whitecaps to develop into maturity in the field and decay slower in seawater may explain the constant temporal and spatial scales found in the experiment of Snyder *et al.* (figure 13) but not in the other laboratory data sets (figures 7, 8, 14–16). The exact nature of flow conditions and chemical properties of the fluid influencing the growth or decay of whitecaps is not well known and outside the scope of this paper.

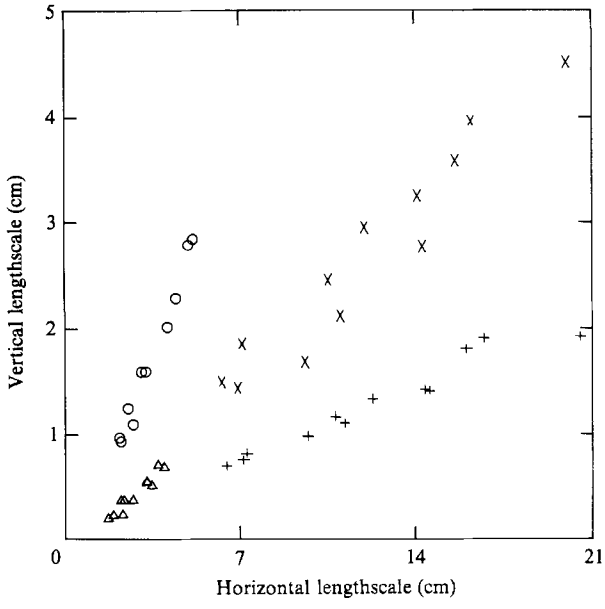

FIGURE 16. Similarity of breaking region as indicated by the linear relationship between the vertical and horizontal lengthscales. Symbols are the same as those in figure 14.

4.5. *Measurement techniques*

The Hilbert transform was used here to derive all the local properties needed for breaking measurements, such as phase velocity, local angular frequency, and surface velocity components. A simpler procedure using the wave period defined by zero up-crossings to calculate the phase velocity and the local steepness was reported by Xu *et al.* (1986). It is interesting to see that their simple method of measurements provided very similar quantitative results for P_b, ΔT_b and ΔH_b to the more elaborate method used here, seen by comparing their figures 3 and 4 with the corresponding figures 4, 7 and 9 in this article. The present method, however, gives an extra option of using different criteria for breaking measurements. Furthermore, direct measurements of acceleration and particle velocity near the surface are very difficult, hindering the application of those variables as breaking criteria. Techniques described in this article provide an accessible means for a detailed description of breaking phenomenon via such breaking parameters.

Comparisons of measurements using local and global parameters were discussed in Xu *et al.* It was shown that for some breaking characteristics, such as breaking probability and the ratio between the height and length of breaking waves, results from local and global parameters agree. Other characteristics, such as the breaking duration and jump height, cannot be easily described by measurements using other global parameters.

4.6. *Breaking criteria*

We have presented measurements of breaking with the critical wave slope and the critical horizontal velocity at the free surface in terms of six breaking characteristics: probability of occurrence, time- and lengthscales of breaking, breaking intensity, phases of breaking, and multiplicity of breaking. All these quantities show strong dependence on the wind velocity, but their dimensionless magnitudes show only weak dependence. The results of our analysis are summarized in table 1. From that

Parameter	Range	Variation with wind velocity
P_b (%)	6.7–66 (1.5–6)	$\begin{cases} u_*^{2.64} (u_* < 80 \text{ cm/s}) \\ u_*^{1.0} (u_* > 80 \text{ cm/s}) \end{cases}$
θ_b (°)	−11–−5 (12–5)	Decreasing with wind
M_b	1–1.2 (1–1.1)	Increasing with wind
ΔT_b (ms)	27–41 (22–23)	$u_*^{0.3}$
ΔL_b (cm)	2–5 (1.7–4)	$u_*^{0.77}$
$\Delta T_b/T_b (= \Delta L_b/L_b)$ (%)	6–4.8 (6.6–3.7)	Weak dependence
ΔH_b (cm)	0.8–2.6 (1.2–0.5)	u_*^1
$\Delta H_b/H_b$ (%)	25–30 (3.6–5.5)	Weak dependence
ΔQ_b (cm^2/s^2)	63–345 (85 ~ 388)	$u_*^{1.34}$
$\Delta Q_b/Q_b$ (%)	20–25 (38 ~ 18)	Weak dependence

TABLE 1. Summary of the breaking characteristics. The first range is based on the geometric criterion, and the second range (in parentheses) on the kinematic criterion. The order of the range is from low to high wind velocity from 7 to 16 m/s.

summary, it is clear that variations with the wind velocity of breaking characteristics determined from the two breaking criteria are qualitatively similar, but the dimensional magnitudes generally differ. The major difference between results determined from geometric and kinematic breaking criteria is in the phase of breaking inception. Although both criteria predict breaking inception near the wave crest, the geometric criterion detects inception on the downwind side, and the kinematic criterion on the upwind side. In terms of the temporal sequence of occurrence, this implies that the geometric instability precedes the kinematic instability. However, such a conclusion from single-point measurements may be biased, a mapping of breaking by an array of instruments is required to resolve this. It suffices to say for now that differences in the measured breaking characteristics, especially the magnitude of breaking height, can be attributed to differences in the phase of inception.

Longuet-Higgins (1985) studied the acceleration field in steep gravity waves. It was shown that the apparent acceleration measured by a fixed wave gauge differs greatly from the real acceleration of fluid particles measured by a Lagrangian device. For monochromatic wavetrains, the real acceleration is generally quasi-sinusoidal even for waves of limited heights. The magnitude of acceleration, either upward or downward, never exceeds $0.39g$. For a more complicated sea, however, Longuet-Higgins proved that the downward true acceleration can be as great as $-g$. On the other hand, although there is generally a maximum upward apparent acceleration ($0.24g$), the magnitude of the downward apparent acceleration follows a delta function for waves of limiting heights. It appears that the delta-function characteristics of the apparent acceleration at the breaking crest is perfect for a 'local' breaking parameter. The difficulty is, however, in the selection of a reasonable threshold. For wind-generated waves, the apparent acceleration calculated from the second derivative of the elevation is quite erratic; this further complicates the application of acceleration as a breaking criterion. It is emphasized here that the acceleration measurements of Ochi & Tsai (1983), Snyder *et al.* (1983) and the present experiment, are made by fixed, stationary probes.

5. Summary and conclusion

The Hilbert transform provides a feasible way of calculating local properties such as phase and particle velocities, surface slopes, particle accelerations, etc. from a single-point measurement of surface elevations. We applied this technique to measurements of breaking waves, and obtained useful quantitative results on breaking characteristics as summarized in table 1. The probability of wave breaking for laboratory-produced wind-generated waves of short-fetch, choppy and chaotic types varies about one decade between low (7 m/s) and high (16 m/s) wind conditions. The breaking duration increases with the wind velocity and ranges between 20 and 40 ms. The non-dimensional breaking duration, normalized by the breaking wave period, is about 0.04 to 0.06, and varies only slightly with the wind velocity. Similarly to the breaking duration, the intensity of breaking expressed as either ΔH_b or ΔQ_b increases with the wind velocity, with the normalized quantities exhibiting less dependence. Occasionally, breaking starting from below the mean water level was observed; this generally was followed by a successive breaking at the most probable phase of inception, within 10° of either side of the wave crest. The probability of multiple breakings in one wave increases with the wind velocity (thus, severity of wave conditions). A detailed comparison with Duncan's (1981) photographic study shows close resemblance of the breaking characteristics derived from temporal and spatial measurements. Linear dependencies of the lengthscales on the flow conditions are identical in his and the present experiments; both indicated a geometrical similarity of the breaking region. Finally, the present technique can be extended to multistation measurements to provide a more complete mapping of breaking events.

We are very grateful for the sponsorship of our work provided by the Fluid Dynamics Program of the Office of Naval Research under Contract N00014-83-K-0316.

REFERENCES

Banner, M. L. & Fooks, E. H. 1985 On the microwave reflectivity of small scale breaking water waves. *Proc. R. Soc. Lond.* A **399**, 93–109.

Banner, M. L. & Melville, W. K. 1976 On the separation of air flow over water waves. *J. Fluid Mech.* **77**, 825–842.

Banner, M. L. & Phillips, O. M. 1974 On the incipient breaking of small scale waves. *J. Fluid Mech.* **65**, 647–656.

Battjes, J. A. & Sakai, T. 1981 Velocity field in a steady breaker. *J. Fluid Mech.* **111**, 421–437.

Bitner-Gregersen, E. M. & Gran, S. 1983 Local properties of sea waves derived from a wave record. *Appl. Ocean Res.* **5**, 210–214.

Blanchard, D. C. & Woodcock, A. H. 1957 Bubble formation and modification in the sea and its meterological significance. *Tellus* **9**, 145–158.

Burger, S. R. & Blanchard, D. C. 1983 The persistence of air bubbles at a seawater surface. *J. Geophys. Res.* **88**, 7724–7726.

Duncan, J. H. 1981 An experimental investigation of breaking waves produced by a towed hydrofoil. *Proc. R. Soc. Lond.* A **377**, 331–348.

Duncan, J. H. 1983 The breaking and non-breaking wave resistance of a two-dimensional hydrofoil. *J. Fluid Mech.* **126**, 507–520.

Gent, P. T. & Taylor, P. A. 1976 A numerical model of the air flow above water waves. *J. Fluid Mech.* **77**, 105–128.

KOGA, M. 1982 Bubble entrainment in breaking wind waves. *Tellus* **34**, 481–489.

LONGUET-HIGGINS, M. S. 1970*a* Longshore currents generated by obliquely incident sea waves. 1. *J. Geophys. Res.* **33**, 6778–6789.

LONGUET-HIGGINS, M. S. 1970*b* Longshore currents generated by obliquely incident sea waves. 2. *J. Geophys. Res.* **33**, 6790–6801.

LONGUET-HIGGINS, M. S. 1974 Breaking waves – in deep or shallow water. In *10th Symp. Naval Hydrodynamics,* pp. 597–605. Office of Naval Research, Arlington, Virginia.

LONGUET-HIGGINS, M. S. 1985 Acceleration in steep gravity waves. *J. Phys. Oceanogr.* **15**, 1570–1579.

LONGUET-HIGGINS, M. S. & FOX, M. J. H. 1977 Theory of the almost-highest wave: the inner solution. *J. Fluid Mech.* **80**, 721–741.

LONGUET-HIGGINS, M. S. & SMITH, N. D. 1983 Measurement of breaking by a surface jump meter. *J. Geophys. Res.* **88**, 9823–9831.

LONGUET-HIGGINS, M. S. & TURNER, J. S. 1974 An 'entraining plume' model of a spilling breaker. *J. Fluid Mech.* **63**, 1–20.

MEDWIN, H. 1977 In situ acoustic measurements of microbubbles at sea. *J. Geophys. Res.* **82**, 971–975.

MELVILLE, W. K. 1977 Wind stress and roughness length over breaking waves. *J. Phys. Oceanogr.* **8**, 702–710.

MELVILLE, W. K. 1983 Wave modulation and breakdown. *J. Fluid Mech.* **128**, 489–506.

MERLIVAT, L. & MEMERY, L. 1983 Gas exchange across an air–water interface: Experimental results and modelling of bubble concentration to transfer. *J. Geophys. Res.* **88**, 707–724.

MICHELL, J. H. 1893 The highest wave in water. *Phil. Mag.* **36** (5), 430–437.

MOGRIDGE, G. R. & JAMIESON, W. W. 1980 Wave impact pressures on composite breakwaters. In *Proc. 17th Coast. Engng Conf.* pp. 1829–1848. ASCE, New York.

MONAHAN, E. C. 1971 Oceanic whitecaps. *J. Phys. Oceanogr.* **1**, 139–144.

MONAHAN, E. C. & ZIETLOW, C. R. 1969 Laboratory comparisons of fresh-water and salt-water whitecaps. *J. Geophys. Res.* **74**, 6961–6966.

OCHI, M. K. & TSAI, C.-H. 1983 Prediction of occurrence of breaking waves in deep water. *J. Phys. Oceanogr.* **13**, 2008–2019.

PEREGRINE, D. H. & SVENDSEN, I. A. 1978 Spilling breakers, bores and hydraulic jumps. In *Proc. 16th Coastal Engng Conf.* pp. 540–551. ASCE, New York.

PHILLIPS, O. M. 1977 *The Dynamics of the Upper Ocean*, 2nd edn. Cambridge University Press.

PHILLIPS, O. M. 1985 Spectral and statistical properties of the equilibrium range in wind-generated gravity waves. *J. Fluid Mech.* **156**, 505–531.

PHILLIPS, O. M. & BANNER, M. L. 1974 Wave breaking in the presence of wind drift and swell. *J. Fluid Mech.* **66**, 625–640.

SNYDER, R. L. & KENNEDY, R. M. 1983 On the formulation of whitecaps by a threshold mechanism Part I: Basic formalism. *J. Phys. Oceanogr.* **13**, 1482–1492.

SNYDER, R. L., SMITH, L. & KENNEDY, R. M. 1983 On the formation of whitecaps by a threshold mechanism. Part III: Field experiment and comparison with theory. *J. Phys. Oceanogr.* **13**, 1505–1518.

SROKOSZ, M. A. 1986 On the probability of wave breaking in deep water. *J. Phys. Oceanogr.* **16**, 382–385.

STIVE, M. J. F. 1980 Velocity and pressure field of a spilling breaker. In *Proc. 17th Coastal Engng Conf.* pp. 547–566. ASCE, New York.

STIVE, M. J. F. & WIND, H. G. 1982 A study of radiation stress and set-up in the nearshore region. *Coastal Engng* **6**, 1–25.

STOKES, G. G. 1880 On the theory of oscillating waves, Appendix B: Considerations relative to the greatest height of oscillatory irrotational waves which can be propagated without change of form. *Math. Phys. Papers* **1**, 225–228.

WIEGEL, R. L. 1982 Forces induced by breaking on piles. In *Proc. 18th Coast. Engng Conf.* pp. 1699–1715. ASCE, New York.

Wu, Jin 1975 Wind-induced drift currents. *J. Fluid Mech.* **68**, 49–70.

Xu, D., Hwang, P. A. & Wu, Jin 1986 Breaking of wind-generated waves. *J. Phys. Oceanogr.* **16**, 2172–2178.

Zheng, Q. A., Klemas, V., Hayne, C. S. & Huang, N. E. 1983 The effect of oceanic whitecaps and foams on pulse-limited radar altimeters. *J. Geophys. Res.* **88**, 2571–2578.